17th World Conference on Earthquake Engineering, 17WCEE
Sendai, Japan - September 13th to 18th 2020

THE EFFECT OF ELASTIC AMPLIFICATION ON ROCKING-INDUCED SEISMIC COLLAPSE OF MASONRY TOWERS

M.J. DeJong [1], A. Mehrotra [2]

[1] *Assistant Professor, Department of Civil and Environmental Engineering – UC Berkeley, dejong@berkeley.edu*
[2] *Postdoctoral Researcher, Department of Civil and Environmental Engineering – UC Berkeley, anjali.a.mehrotra@gmail.com*

Abstract

Seismic collapse mechanisms for masonry structures are consistent and well documented. Engineers often assess these mechanisms using simplified limit analysis, while researchers assess them using complicated computational modeling. However, limit analysis can underestimate dynamic capacity and lead to expensive retrofitting solutions, while most numerical strategies can be computationally demanding. Meanwhile, the use of rocking dynamics to evaluate collapse can preserve the simplicity of limit analysis while improving assessment accuracy by incorporating the dynamics of the response.

Previous research focused on the development of tools to assess rocking-induced collapse using a supplied ground motion. However, in many tall slender structures, amplification of the ground motion cannot be neglected when evaluating mechanisms that occur well above the ground. Quantifying amplification requires estimation of mode shapes and natural frequencies, creating undesired computational burden for geometrically complex structures.

In this context, a new modelling strategy was developed that combines finite element analysis with rocking dynamics to evaluate seismic collapse in a computationally efficient manner. As input, the framework requires a 3D CAD model of the structure, material properties, geometric definition of the collapse mechanism to be assessed, and the ground motion. The simplicity of the approach is preserved by automatic generation of a corresponding FE model, and an automated procedure that uses modal analysis to determine the input seismic signal at the base of the mechanism.

In this paper, the new tool is used to evaluate the importance of elastic amplification when assessing the capacity of masonry towers to resist seismic collapse. Using only tower geometries and expected collapse mechanisms as input, parametric studies are conducted on three Italian masonry towers to assess the effects of boundary conditions on the dynamic capacity of the structures. The parametric models are subjected to a suite of ground motions and the rocking response of each of the mechanisms is compared. From these analyses it is found that for the level of seismic hazard expected on site, overturning failure is unlikely to occur for all but one of the mechanisms. The boundary conditions are also observed to influence the level of amplification and frequency content of the filtered ground motion, with lower frequencies proving to be more destructive for the rocking response.

Keywords: rocking dynamics; elastic amplification; masonry collapse mechanisms; computational tools

1. Introduction

Failure of masonry structures under the influence of seismic action often occurs via consistent, well-documented collapse mechanisms [1], [2]. Assessment of these collapse mechanisms can be conducted using either simplified limit analysis, or through the use of more complex computational modelling strategies such as finite element analysis or discrete element methods. However, limit analysis tends to underestimate dynamic capacity - leading to expensive and occasionally unnecessary retrofitting solutions, while most numerical modelling strategies can be computationally expensive – especially when modelling collapse. Alternatively, rocking dynamics, whereby equations of motion describing predefined collapse mechanisms are directly derived and solved, can be used instead [3]–[5]. Such an approach preserves the simplicity of limit analysis while simultaneously improving assessment accuracy through incorporation of the dynamics of the response.

In this context, previous research focused on the development of a framework to assess rocking-induced collapse using a supplied ground motion [6]. However, in the case of tall slender structures such as masonry towers, elastic amplification effects cannot be neglected – particularly in the case of mechanisms which take place well above ground level. In order to quantify this amplification, mode shapes and natural frequencies of the structures need to be estimated [7], which in the case of complex structural geometries often requires generation of a finite element (FE) model for analysis, creating undesired computational burden.

To this end, a new integrated modelling strategy has been developed which combines finite element analysis with rocking dynamics in order to evaluate seismic collapse in a computationally-efficient manner [8]. As input, the new framework requires only a 3D CAD model of the structure, basic material properties (Young's modulus, Poisson's ratio and density), geometric definition of the collapse mechanism(s) to be assessed and the ground motion at the base of the structure. Once this data has been provided, the framework calculates the equivalent rocking parameters defining the equation of motion for each of the different collapse mechanisms, all of which depend entirely on the geometry of the structure as expounded upon in [6]. Depending on the heights at which the mechanisms occur, the tool then automatically generates the corresponding FE model and conducts modal analyses to determine the resultant filtered and scaled seismic signals, which in turn serve as input at the base of the different rocking mechanisms.

In this paper, the new tool is used to evaluate the influence of elastic amplification on the seismic capacity of masonry towers. Three towers from northeastern Italy are used as case studies, and models are created for a predefined set of collapse mechanisms with varying boundary conditions. The models are subjected to a suite of ground motions, comprising both pulse and non-pulse-type records, and the rocking response of each of the mechanisms is compared. From these comparisons, conclusions are drawn about the overturning vulnerability of the mechanisms, and the extent to which the rocking response is influenced by the boundary conditions through their impact on the amplification and filtering of the input ground motion.

2. Methodology

2.1 Geometric description of the three towers

The three towers chosen for this study are illustrated by Fig.1. The first tower (Tower 1, Fig.1a) selected for analysis is the bell tower of San Giacomo church, found in the town of Polesine, Mantua. The tower is constructed of clay bricks, with a height of 25.5 m and dimensions of 4.6 × 4.6 m at the base, which gradually tapers to 3.8 × 3.8 m in the belfry due to the diminishing thickness of the walls – which in turn taper from 80 cm at the bottom of the structure to 40 cm near the top [9]. The tower is freestanding, i.e. completely separated from the church, thus ruling out the possibility of any type of dynamic interaction between the two structures [9]. Small openings are present on all four façades, with larger arched openings present in the belfry.

The second tower (Tower 2, Fig.1b) considered in this study is a clock tower found in the town of Lendinara, Veneto. Similar to Tower 1, it is approximately square in plan and constructed entirely in brick, with a height of 25.7 m and base dimensions of 7.2 × 8.0 m [9]. The walls are roughly 100 cm thick for the bottom 12.6 m, with this thickness reducing to 50 cm near the top [9]. Two large arches are present on the

eastern and western façades at the bottom of the structure, which enable the tower to connect the two small squares that it borders [9]. Unlike Tower 1, part of the northern and southern façades appear to be connected to the adjacent buildings. All four façades have large double openings at the upper level of the structure, with merlon (rampart) elements present at the very top [9].

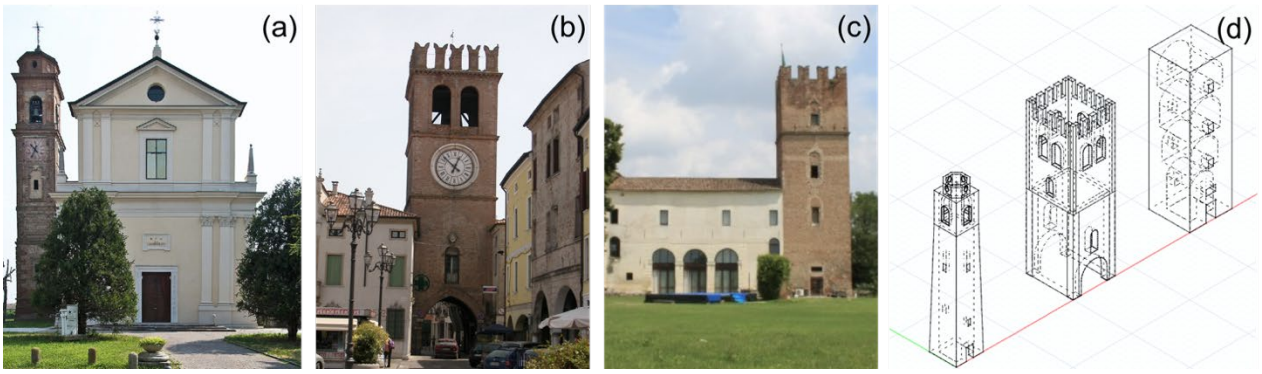

Fig. 1 – Towers selected for analysis: (a) Tower 1 (t1) - Bell tower of San Giacomo church (far left, Chiese Italiane), (b) Tower 2 (t2) - Clock tower in Lendinara (Wikimedia Commons), (c) Tower 3 (t3) - Tower of Treves Castle (far right, Luigi Prearo) and (d) Rhino/CAD models of the three towers

The third and final tower selected for analysis (Tower 3, Fig.1c) corresponds to the tower of Treves Castle, located in the town of Arqua Polesine, Veneto. As in the case of Towers 1 and 2, this tower is also square in plan, with base dimensions of 7.2 × 7.2 m and a height of 23.8 m [9]. Internally the structure is subdivided into four tiers, with each tier comprising a square room with a barrel-vaulted ceiling [9]. Wall thickness varies from tier to tier, with thicknesses of 160 cm, 120 cm, 100 cm and 80 cm on the ground, first, second and third floors respectively [9]. Small openings in the form of windows and a door are present on the northern and southern façades, while part of the western façade is connected to the adjoining castle.

Using the above information as well as plan and elevation drawings as found in the literature [9], 3D models were then generated in the CAD software Rhino for each of the three towers as illustrated by Fig.1d.

2.2 Definition of collapse mechanisms for rocking analysis

2.2.1 Tower 1

In the case of Tower 1, three different collapse mechanisms were selected for analysis - all of which involve the belfry, as illustrated by Fig. 2. These mechanisms occur high enough up the structure so that amplification effects may be important. While mechanisms 1a and 1b involve corner failure, with cracks originating at the opening of the belfry, mechanism 2 is a variation of the symmetric rocking portal frame. In the case of the corner mechanisms, the crack angles were chosen to represent both an average value (α_c = 45º, 1a) as well as an upper limit (α_c = 70º, 1b) for a range of different brick aspect ratios and bonding patterns [10].

Once the collapse mechanisms (and their corresponding axes of rotation) have been defined in Rhino, the tool then calculates the equivalent rocking parameters defining their corresponding equations of motion, which for the simple single block mechanism assumes the following general linearized form:

$$\ddot{\phi} = p_{eq}^2 \left(\phi - \lambda - \frac{\ddot{u}_g}{g} \right) \tag{1}$$

where ϕ is the rotation of the block, p_{eq} is the rocking frequency parameter, λ is an approximation of the static load multiplier which activates the mechanism and $\ddot{u}_g$ is the input ground acceleration normalized by the acceleration due to gravity g. In addition to p_{eq} and λ, the other rocking parameters include the overturning rotation ϕ_{ov} (upon the exceedance of which the part of the structure involved in the rocking mechanism will collapse), as well as the coefficient of restitution η which provides a measure of the energy dissipated by the block(s) during impact and depends in turn on whether the mechanism is undergoing one-sided or two-sided

rocking (indicated by the parameter *ns*). The final rocking parameter required for the analysis is the mechanism height h_m, which corresponds to the height of the axis of rotation, and which is used to scale the input ground motion as expounded upon in [8]. Table 1 lists the equivalent rocking parameters as computed by the tool for the various collapse mechanisms considered for Tower 1.

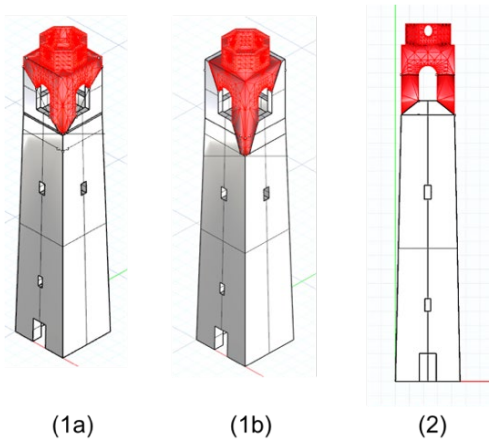

Fig. 2 – Tower 1 collapse mechanisms selected for analysis: (1a) corner failure with a crack angle $\alpha_c = 45^o$, (1b) corner failure with a crack angle $\alpha_c = 70^o$ and (2) symmetric portal frame mechanism

Table 1 – Equivalent rocking parameters for the different Tower 1 mechanisms

	p_{eq} (s^{-1})	λ (rad)	ϕ_{ov} (rad)	*ns*	η	h_m (m)
t1_m1a	1.33	0.49	0.49	1	-0.14	19.15
t1_m1b	1.22	0.34	0.34	1	-0.38	17.66
t1_m2	1.04	0.76	0.62	2	0.90	19.00

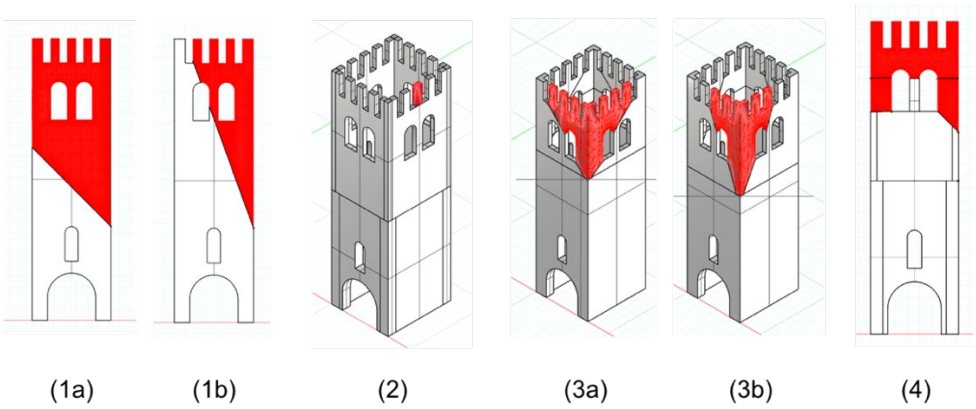

Fig. 3 – Tower 2 collapse mechanisms selected for analysis: (1a) overturning failure with a crack angle $\alpha_c = 45^o$, (1b) overturning failure with a crack angle $\alpha_c = 70^o$, (2) single-block rampart overturning, (3a) corner failure with a crack angle $\alpha_c = 45^o$, (3b) corner failure with a crack angle $\alpha_c = 70^o$ and (4) asymmetric portal frame mechanism

2.2.2 Tower 2

In the case of Tower 2, five different collapse mechanisms were selected for analysis as illustrated by Fig. 3. Mechanisms 1a and 1b arise from the development of large diagonal cracks across the structure, while mechanism 2 involves overturning of one of the rampart elements at the very top of the tower. Mechanisms 3a and 3b involve corner failure, with cracks originating at the large double openings, while mechanism 4 is a variation of the asymmetric portal frame. In the case of mechanisms 1 and 3, the crack angles were once again selected to represent both an average value (α_c = 45º, 1/3a) as well as an upper limit (α_c = 70º, 1/3b) for a range of different brick aspect ratios and bonding patterns. The equivalent rocking parameters as computed by the tool for each of these different mechanisms can be found in Table 2.

Table 2 – Equivalent rocking parameters for the different Tower 2 mechanisms

	p_{eq} (s^{-1})	λ (rad)	ϕ_{ov} (rad)	*ns*	η	h_m (m)
t2_m1a	0.89	0.30	0.30	1	-0.27	8.55
t2_m1b	0.92	0.11	0.11	1	-0.50	8.55
t2_m2	2.55	0.22	0.22	2	0.93	23.50
t2_m3a	1.22	0.33	0.33	1	-0.35	17.10
t2_m3b	1.12	0.20	0.20	1	-0.56	15.00
t2_m4 (+)	0.91	0.60	0.55	2	0.90	16.60
t2_m4 (-)	1.01	0.96	0.61	2	0.90	18.30

2.2.3 Tower 3

Finally in the case of Tower 3, four different collapse mechanisms were selected for analysis as illustrated by Fig.4. All considered mechanisms are variations of single block overturning failure, with the mechanisms developing due to large diagonal cracks originating at one or more of the window openings. As in the case of Towers 1 and 2, the crack angles were selected to represent both an average value (α_c = 45º, 1a/b) as well as an upper limit (α_c = 70º, 1c/d) to account for uncertainties associated with the brick aspect ratio and bonding pattern. Table 3 lists the equivalent rocking parameters computed by the tool for these different mechanisms.

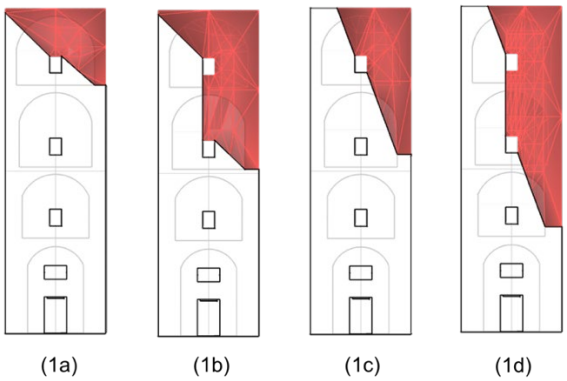

Fig. 4 - Tower 3 collapse mechanisms selected for analysis. Overturning failure with: (1a) cracks originating at the first window with crack angles α_c = 45º, (1b) cracks originating at the first and second windows with crack angles α_c = 45º, (1c) cracks originating at the first window with crack angles α_c = 70º and (1d) cracks originating at the first and second windows with crack angles α_c = 70º

Table 3 – Equivalent rocking parameters for the different Tower 3 mechanisms

	p_{eq} (s^{-1})	λ (rad)	ϕ_{ov} (rad)	ns	η	h_m (m)
t3_m1a	1.27	0.56	0.56	1	-0.03	18.20
t3_m1b	1.02	0.28	0.28	1	-0.34	12.20
t3_m1c	1.09	0.21	0.21	1	-0.43	13.13
t3_m1d	0.92	0.16	0.16	1	-0.47	7.68

2.3 Modal analyses

As all considered mechanisms take place above ground level ($h_m > 0$), finite element models of the three towers were automatically generated by the tool and modal analyses conducted. The results of these analyses were used to transform the structures into equivalent single-degree-of-freedom (SDF) elastic oscillators – which in turn are used to account for the amplification and filtering of the ground motion by the structures in a simplified manner. The material properties assumed for all models were that of an elastic isotropic material characterised by a Young's modulus $E = 0.84$ GPa, a Poisson's ratio $\upsilon = 0.2$ and density $\rho = 2000$ kg/m^3.

As Tower 1 is freestanding, only one FE model of the structure needed to be generated. However, in the case of Tower 2, the bottom 8.55 m of the structure is connected to adjacent buildings on the northern and southern façades, with limited information available about the type/level of connectivity. Therefore, two different boundary conditions were considered to provide a lower and upper bound. These are the isolated case (zero connectivity to the adjacent structures) and the fixed case (tower completely restrained, i.e. pinned, to the adjacent structures). Similarly in the case of Tower 3, the bottom 11.2 m of its western façade is connected to the adjacent castle, but again with limited information available about the connection quality. Both isolated and fixed case models were considered for this tower as well. The results of the modal analyses were then used to define equivalent SDF elastic oscillators characterised by the natural frequencies indicated in Table 4.

Table 4 – Natural frequencies of the three towers for the different boundary conditions

	Tower 1		**Tower 2**		**Tower 3**	
f_n (Hz)	**Mode 1**	**Mode 2**	**Mode 1**	**Mode 2**	**Mode 1**	**Mode 2**
isolated	1.13	1.17	1.53	1.58	1.39	1.45
fixed	-	-	2.70	2.78	2.75	2.86

2.4 Full time-history analyses

Full time-history analyses were subsequently conducted in order to gauge the response of the structures/mechanisms to a suite of earthquake ground motions. Using the PEER NGA-West2 ground motion database, 15 different ground motions (comprising a mix of pulse and non-pulse type records) were selected for analysis, scaled to the site-specific response spectrum as defined in Eurocode 8 assuming soil type C – and as illustrated by Fig.5. As all three towers are located in a zone of low/medium seismicity, with a maximum PGA of 0.075 – 0.125g expected with a 10% probability of exceedance in 50 years, the ground motion applied to the towers was consequently scaled to PGA = 0.1g (or some factor thereof) to gauge the vulnerability of the structures to collapse.

The equivalent SDF elastic oscillators as defined in the previous subsection were then solved for each of the ground motions, and the filtered response scaled to get the final input signals at the base of the different rocking mechanisms. These filtered and scaled input signals were finally substituted into Eq. (1), which was

solved to predict the response of each of the collapse mechanisms to the different ground motions, for both the isolated and fixed cases (where relevant), with the predictions expressed in terms of rotation ϕ over time.

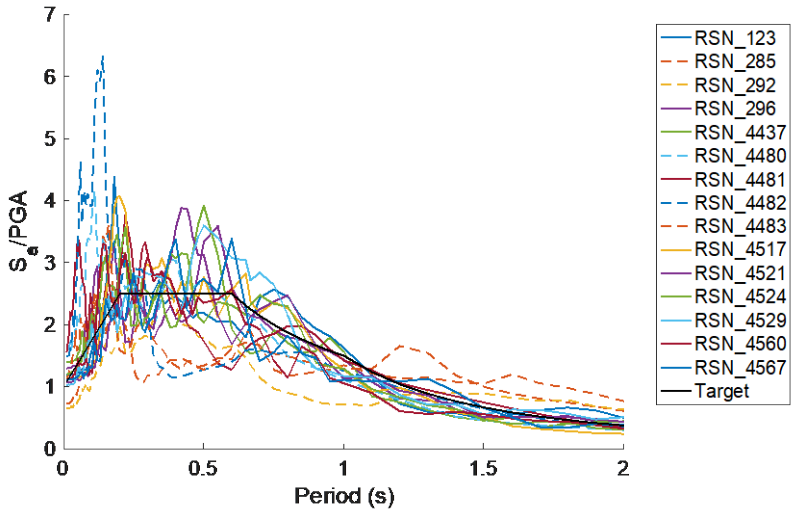

Fig. 5 – Elastic acceleration spectra (normalized by PGA) of the ground motions selected for analysis, with the site-specific target spectrum shown in black, pulse-type records indicated by dashed lines and non-pulse type records by solid lines

3. Results

3.1 Tower 1

In the case of Tower 1, all three collapse mechanisms were analyzed simultaneously. For each of the collapse mechanisms, the maximum predicted rotation ϕ_{max} (normalized by the overturning rotation ϕ_{ov}) was compared for each of the different ground motion records, scaled in this case to a PGA = 0.5g in order for rocking to initiate for all three mechanisms. As Fig.6 illustrates, mechanism t1_m1b appears to be the most vulnerable of the three – due in part to being the most slender - consistently experiencing the largest rotations and overturning for 2 of the 15 ground motion records. Overturning in this paper is defined as taking place when $\phi_{max}/\phi_{ov} = 1$ - although failure would occur at lower rotations in reality. For the entire suite of earthquake ground motions, ϕ_{max}/ϕ_{ov} is found to have a median value of 0.56 for t1_m1b, and median values of 0.34 and 0.16 for t1_m1a and t1_m2 respectively.

3.2 Tower 2

In the case of Tower 2, the first set of analyses were conducted on mechanisms t2_m1a and t2_m1b, for both the isolated ("iso") and fixed ("fix") cases in order to better understand the influence of different boundary conditions on dynamic response. As in the case of Tower 1, the ground motion was once again scaled to a PGA = 0.5g in order for rocking to initiate for all considered mechanisms. As Fig.7 illustrates, the isolated case of mechanism t2_m1b displays the highest vulnerability to collapse, overturning for 12 of the 15 ground motion records and resulting in a median ϕ_{max}/ϕ_{ov} value of 1.00. Meanwhile, the fixed case of t2_m1b results in a median ϕ_{max}/ϕ_{ov} value of 0.10, which is comparable to the median ϕ_{max}/ϕ_{ov} value of 0.11 recorded for the isolated case of t2_m1a – indicating that the benefits of fixing the boundary conditions for t2_m1b are akin to decreasing the slenderness of the mechanism (from $\lambda = 0.30$ to $\lambda = 0.11$). The fixed case of t2_m1a on the other hand records the smallest - almost imperceptible - rotations, resulting in a median ϕ_{max}/ϕ_{ov} value of 0.004.

In the case of mechanism t2_m2, analyses were conducted using both the isolated and fixed case models, with the ground motion scaled to a PGA = 0.1g, which corresponds to the actual maximum PGA expected on site. As Fig.8 illustrates, for this level of scaling of the earthquake ground motion, the isolated model fails via overturning for 4 of the15 ground motion records, with a median ϕ_{max}/ϕ_{ov} value of 0.71 for the entire suite. For

the fixed case the predictions of the rocking equation of motion are once again far lower (with the exception of RSN 4437 where the two are identical), with a median ϕ_{max}/ϕ_{ov} value of 0.30 for the entire suite.

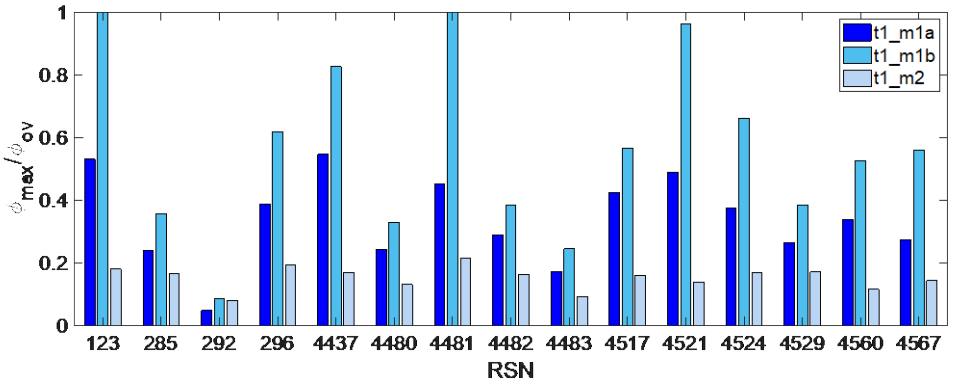

Fig. 6 – Maximum rotation ϕ_{max} (normalized by overturning rotation ϕ_{ov}) recorded for each of the different ground motion records (scaled to a PGA = 0.5g), for the various Tower 1 mechanisms

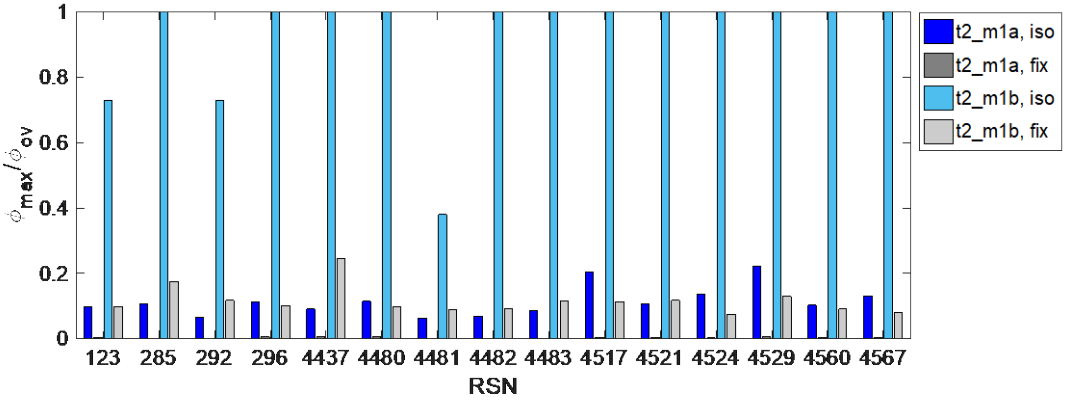

Fig. 7 – Tower 2 mechanisms (1a) and (1b): maximum rotation ϕ_{max} (normalized by overturning rotation ϕ_{ov}) recorded for each of the different ground motion records (scaled to a PGA = 0.5g), for both the isolated and fixed cases

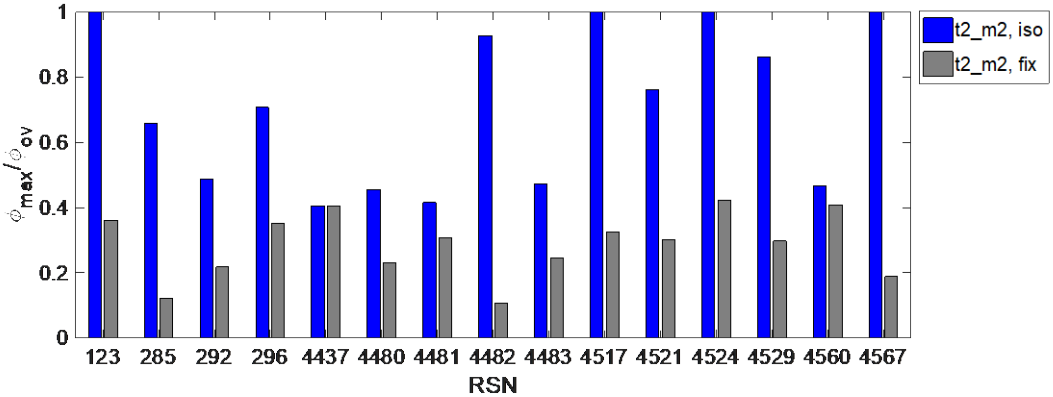

Fig. 8 – Tower 2 mechanism 2: maximum rotation ϕ_{max} (normalized by overturning rotation ϕ_{ov}) recorded for each of the different ground motion records (scaled to a PGA = 0.1g), for both the isolated and fixed cases

The next set of analyses were conducted on mechanisms t2_m3a and t2_m3b, with the ground motion scaled to a PGA = 0.5g to initiate rocking for the stockier mechanism t2_3b. The results of these analyses are presented in Fig.9 for both the isolated and fixed cases. As Fig.9 illustrates, this level of ground motion scaling results in failure via mechanism t2_m3a for 5 of the 15 records and via t2_m3b for 13 of the 15 records for the isolated case, with median ϕ_{max}/ϕ_{ov} values of 0.56 and 1.00 respectively. It is clear that in this case the

slenderness of t2_m3b (λ = 0.20, as opposed to λ = 0.33 for t2_m3a) controls the response, resulting in overturning of t2_m3b more frequently than t2_m3a – despite the fact that both mechanisms are of similar scale, with t2_m3a also occurring slightly higher up than t2_m3b and consequently experiencing a greater degree of amplification. Similarly, for the fixed case, t2_m3a experienced smaller average median ϕ_{max}/ϕ_{ov} values than t2_m3b (0.09 and 0.16 respectively). As in the case of the previously considered mechanisms for this tower, the predictions for the fixed case are also considerably less conservative than their isolated counterparts.

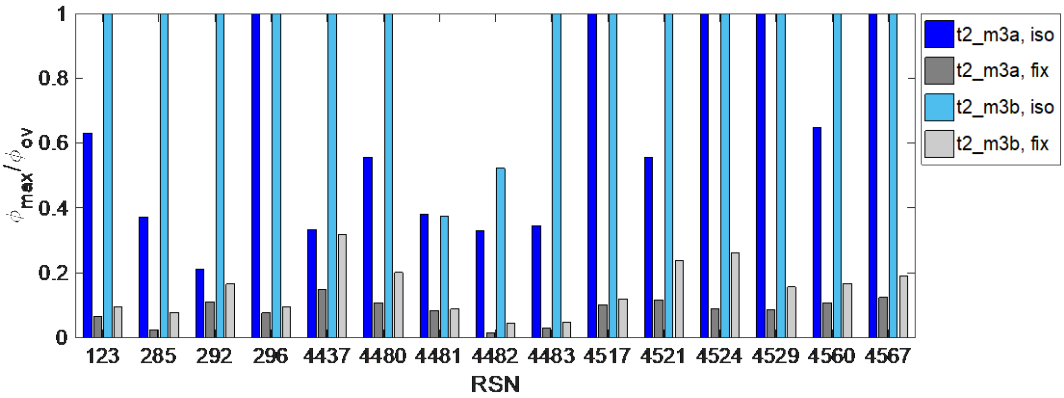

Fig. 9 – Tower 2 mechanisms (3a) and (3b): maximum rotation ϕ_{max} (normalized by overturning rotation ϕ_{ov}) recorded for each of the different ground motion records (scaled to a PGA = 0.5g), for both the isolated and fixed cases

The final set of analyses for Tower 2 were conducted on mechanism t2_m4 (the asymmetric portal frame). To demonstrate the importance of accounting for amplification effects, the analyses conducted now also include the case of no ground motion amplification (in addition to the isolated and fixed cases). Due to the relatively stocky nature of this mechanism, the ground motion had to be scaled to a PGA = 1.0g in order for rocking to initiate. As Fig.10 illustrates, neglecting amplification effects results in significantly smaller predicted rotations (median ϕ_{max}/ϕ_{ov} = 0.04) compared to the isolated (median ϕ_{max}/ϕ_{ov} = 0.34) and fixed (median ϕ_{max}/ϕ_{ov} = 0.12) cases, thus underlining the importance of accounting for these effects.

3.3 Tower 3

In the case of Tower 3, all four collapse mechanisms were assessed simultaneously, with the results presented separately for the isolated and fixed cases (Figs.11 and 12, respectively). The ground motion in this case was scaled to a PGA = 0.5g in order for rocking to initiate for all four mechanisms.

As Fig.11 illustrates, if the tower is assumed to be freestanding, failure is most likely to occur via mechanism t3_m1c - with the tool actually predicting collapse of this mechanism for one of the ground motion records (RSN 4529) and a median value of ϕ_{max}/ϕ_{ov} = 0.28 for the entire suite. Note that this is double the median maximum rotation predicted for the other mechanisms, with median ϕ_{max}/ϕ_{ov} values of 0.15, 0.13 and 0.12 being recorded for mechanisms t3_1a, t3_1b and t3_1d respectively. The similarities in response for mechanisms t3_1a and t3_1b in particular could be attributed to the trade-off between amplification and mechanism slenderness. While t3_1a takes place at a height of 18.20 m and experiences an average maximum acceleration of 1.78g at its base, due to its relatively low slenderness (λ = 0.56) it undergoes rotations of a similar magnitude to t3_1b which is twice as slender (λ = 0.28) but experiences slightly more than half the maximum base acceleration (0.93g).

On the other hand, if the tower is assumed to be fixed to the adjacent castle, all four mechanisms experience similarly small rotations, with median ϕ_{max}/ϕ_{ov} values in the range of 0.01 to 0.04. In the case of mechanism t3_1d in particular, it was observed that despite the isolated and fixed models both experiencing similar average maximum accelerations at their bases (0.55g and 0.58g respectively), the fixed case model records a median ϕ_{max}/ϕ_{ov} value of 0.04 – almost a third of the value recorded by its isolated counterpart.

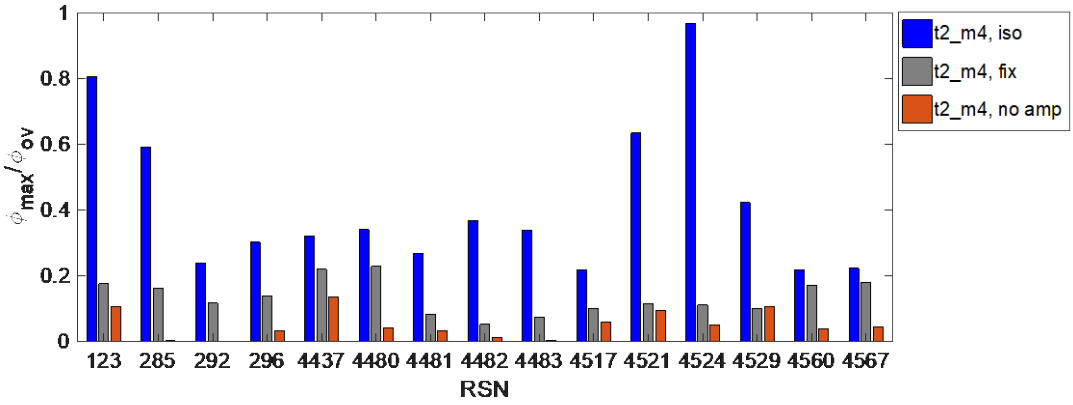

Fig. 10 – Tower 2 mechanism 4: comparison of the maximum rotation ϕ_{max} (normalized by overturning rotation ϕ_{ov}) recorded for each of the different ground motion records (scaled to a PGA = 1.0g), for the isolated, fixed and no amplification cases

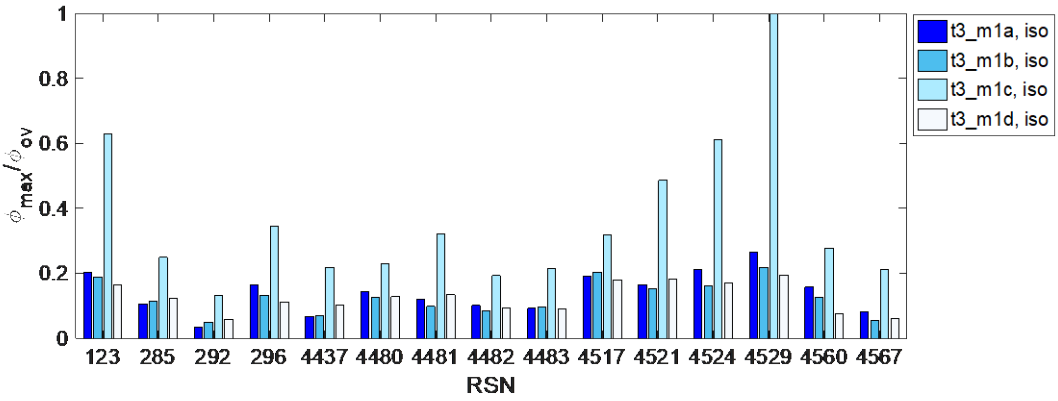

Fig. 11 – Tower 3, all mechanisms: maximum rotation ϕ_{max} (normalized by overturning rotation ϕ_{ov}) recorded for each of the different ground motion records (scaled to a PGA = 0.5g), for the isolated case only

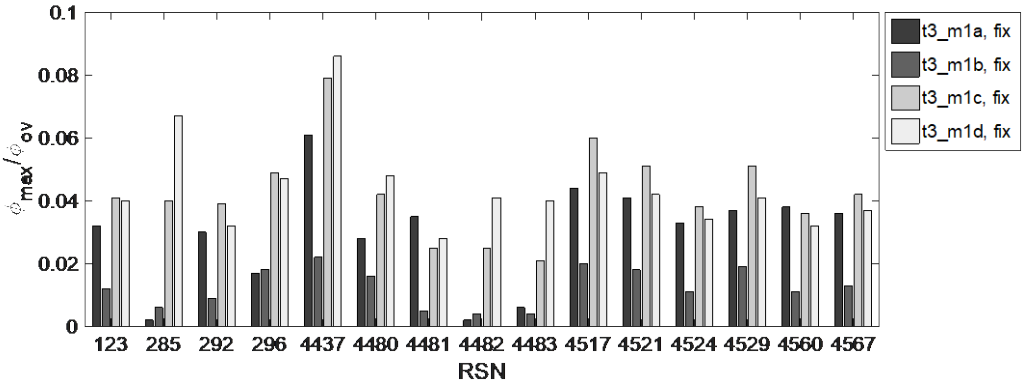

Fig. 12 – Tower 3, all mechanisms: maximum rotation ϕ_{max} (normalized by overturning rotation ϕ_{ov}) recorded for each of the different ground motion records (scaled to a PGA = 0.5g), for the fixed case only

4. Discussion

4.1 Influence of boundary conditions on dynamic response

As the previous section demonstrates, the models with fixed boundary conditions consistently appear to record smaller displacements than their isolated counterparts. This is due in part to the extent of amplification

experienced by the ground motion, which depends in turn on the frequency of the structure. As Fig.13a and Table 4 illustrate, the towers with isolated boundary conditions have lower natural frequencies than their fixed counterparts. In the case of the three towers considered in this paper, this generally results in a lower initial elastic amplification (Fig.13a). However, the initial response is computed at the effective modal height h_e which then needs to be scaled to the mechanism height h_m using the ratio u(h_m)/u(h_e) as extracted from the mode shape (shown here in Fig.13b for Tower 2). For most mechanisms considered in this study, this ratio is generally larger for the isolated case than the fixed case, resulting in a greater magnitude of acceleration being experienced at the base of the isolated case mechanisms.

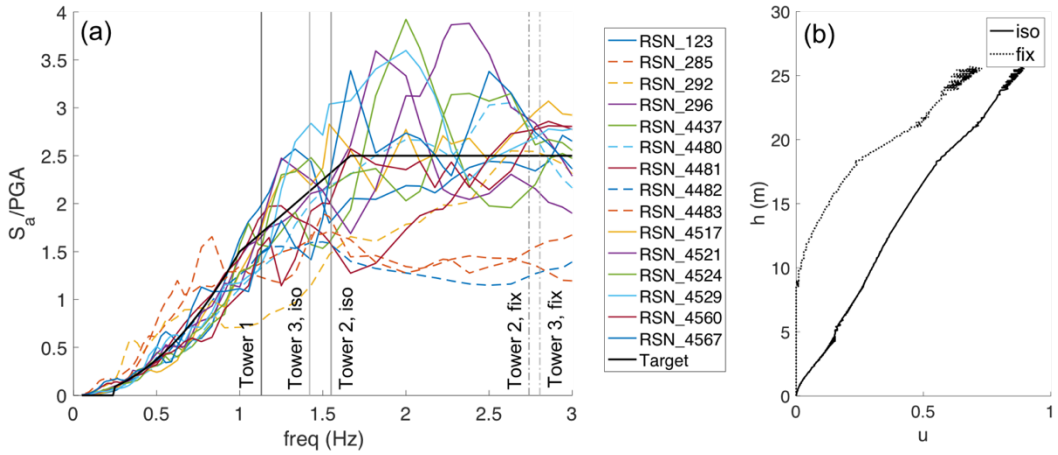

Fig. 13 – Influence of boundary conditions on: (a) intial elastic amplification of the ground motion and (b) variation of amplification with height for Tower 2 (mode shape)

Furthermore, the isolated and fixed boundary conditions also influence the frequency at which the structure responds to the initial input ground motion – with the filtered accelerations experienced at the base of the rocking mechanisms having a frequency content similar to that of the natural frequency of the structure. As the isolated case generally has a lower frequency than its fixed counterpart, its filtered ground motion is consequently more destructive for the rocking mechanism. This is why in the case of mechanism t3_1d, despite similar magnitudes of acceleration being experienced at the base of the mechanism, the isolated model results in rotations that are three times as large as those of the fixed model.

4.2 Practical implications

In order to determine the actual susceptibility of the various mechanisms considered in this study to collapse, the analyses were re-run with the ground motions scaled to a PGA = 0.2g, thereby providing a safety factor of

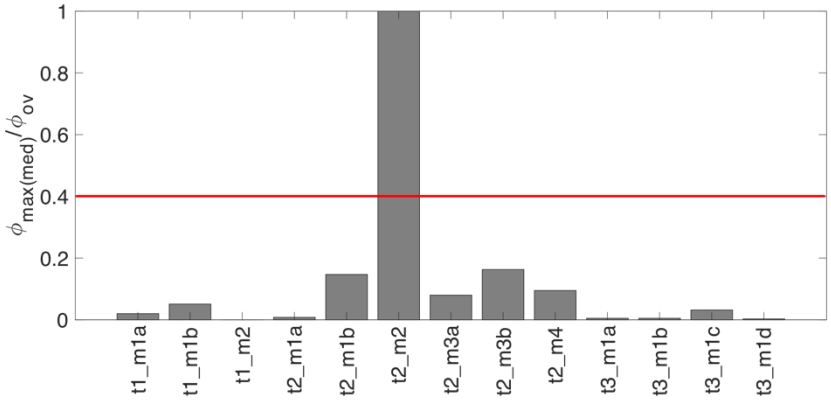

Fig. 14 – Comparison of the median maximum rotations $\phi_{max(med)}$ normalized by the overturning rotation ϕ_{ov} for all considered mechanisms, for ground motion that has been scaled to a PGA = 0.2g

2 on the maximum expected PGA on site. The median ϕ_{max}/ϕ_{ov} values for each of the mechanisms were then compared in order to determine the relative vulnerabilities of the different mechanisms to collapse.

As Fig.14 illustrates, for this level of scaling of the earthquake ground motion, only t2_m2 (single-block rampart mechanism) is in danger of failure via overturning collapse. The next two largest responses are of mechanisms t2_m1b (single block with a large diagonal crack, $\alpha_c = 70^o$) and t2_m3b (corner failure, $\alpha_c = 70^o$). However these responses are significantly smaller than those of t2_m2, with median ϕ_{max}/ϕ_{ov} values of 0.15 and 0.16 respectively – which are also only about 40% of the allowable rotation specified by the Italian building code ($\phi_{max}/\phi_{ov} = 0.4$, as indicated by the solid red line in Fig.14) [11].

5. Conclusions

In this paper, a new modelling tool for the seismic collapse assessment of masonry structures is used to evaluate the dynamic response of three historic towers in northeastern Italy. The new modelling strategy integrates rocking dynamics with finite element analysis to model the response of these complex structural geometries in a computationally-efficient manner.

Through a series of full time-history analyses conducted using a suite of different earthquake ground motions, it was found that the boundary conditions assumed for the towers had a substantial influence on dynamic behavior – both in terms of the extent of amplification as well as the frequency content of the filtered records, which in turn affected the rocking response of the assumed mechanisms. Comparison with results of analyses where elastic amplification had not been considered at all further underscored the importance of accounting for these effects. It was finally concluded that for the level of seismic hazard expected on site, only one of the towers is vulnerable to minor local collapse via overturning of one of its rampart elements.

6. References

[1] D'Ayala D, Speranza E (2002): An Integrated Procedure for the Assessment of Seismic Vulnerability of Historic Buildings. *12th European Conference on Earthquake Engineering*, London, UK.

[2] PCM-DPC MiBAC (2006): Model A-DC Scheda per il rilievo del danno ai beni culturali - Chiese.

[3] Housner GW (1963): The Behavior of Inverted Pendulum Structures during Earthquakes. *Bulletin of the Seismological Society of America*, **53**(2), 403–417.

[4] Mauro A, de Felice G, DeJong MJ (2015): The relative dynamic resilience of masonry collapse mechanisms. *Engineering Structures*, **85**, 182–194.

[5] DeJong MJ, Dimitrakopoulos EG (2014): Dynamically equivalent rocking structures. *Earthquake Engineering & Structural Dynamics*, **43**(10), 1543–1563.

[6] A. Mehrotra and M. J. DeJong (2018): A CAD-interfaced dynamics-based tool for analysis of masonry collapse mechanisms. *Engineering Structures*, **172**, 833–849.

[7] Priestley MJN (1985): Seismic behaviour of unreinforced masonry walls. *Bulletin of the New Zealand Society for Earthquake Engineering*, **18**(2), 191–205.

[8] Mehrotra A, Liew A, Block P, DeJong MJ (2020): An integrated modeling approach that combines elastic amplification and rocking analysis for seismic assessment of a masonry tower. *12th International Conference on Structural Analysis of Historical Constructions (SAHC 2020)*, Barcelona, Spain.

[9] Valente M, Milani G (2016): Seismic assessment of historical masonry towers by means of simplified approaches and standard FEM. *Construction and Building Materials,* **108**, 74–104.

[10] Malomo D, DeJong MJ, Penna A (2019): Influence of bond pattern on the in-plane behavior of URM piers. *International Journal of Architectural Heritage.*

[11] DMI (2008): Approvazione delle nuove norme tecniche per le costruzioni. G.U. no. 29, Suppl. Ord n. 30.

